Removal of triclosan from water by adsorption on activated carbons and photodegradation

Nahum Andrés Medellin-Castillo (nahum.medellin@uaslp.mx)
Universidad Autonoma de San Luis Potosi https://orcid.org/0000-0001-9245-8016
Lázaro Adrián González-Fernández
Autonomous University of San Luis Potosi: Universidad Autonoma de San Luis Potosi
Raúl Ocampo-Pérez
Universidad Autónoma de San Luis Potosí: Universidad Autonoma de San Luis Potosi
Roberto Leyva-Ramos
Universidad Autónoma de San Luis Potosí: Universidad Autonoma de San Luis Potosi
Guilherme Luiz-Dotto
Universidade Federal de Santa Maria
Rogelio Flores Ramírez
Universidad Autónoma de San Luis Potosí: Universidad Autonoma de San Luis Potosi
Amado Enrique Navarro-Frómeta
Universidad Tecnológica de Izúcar de Matamoros: Universidad Tecnologica de Izucar de Matamoros
Miguel Mauricio Aguilera-Flores
Instituto Politécnico Nacional: Instituto Politecnico Nacional
Francisco Carrasco-Marín
Universidad de Granada
Héctor Hernández-Mendoza
Universidad Autónoma de San Luis Potosí: Universidad Autonoma de San Luis Potosi
Samuel Aguirre-Contreras
Universidad Autónoma de San Luis Potosí: Universidad Autonoma de San Luis Potosi

Research Article

Keywords: Triclosan, activated carbons, photodegradation, adsorption, emerging pollutants, radicals

Posted Date: March 23rd, 2022

DOI: https://doi.org/10.21203/rs.3.rs-1440179/v1

Removal of triclosan from water by adsorption on activated carbons and photodegradation

Lázaro Adrián González-Fernández[a,b], Nahum Andrés Medellín-Castillo[a,b*],Raúl Ocampo-Pérez[c], Roberto Leyva Ramos[c], Guilherme Luiz-Dotto[d], Rogelio Flores Ramírez[e], Amado Enrique Navarro-Frómeta[f], Miguel Mauricio Aguilera-Flores[b,g], Francisco Carrasco-Marín[h], Héctor Hernández-Mendoza[i], Samuel Aguirre-Contreras[c]

[a]*Faculty of Engineering, Autonomous University of San Luis Potosi, Av. Dr. Manuel Nava No. 8, Zona Universitaria, 78290, San Luis Potosi, SLP, Mexico*

[b]*Autonomous University of San Luis Potosi, Multidisciplinary Graduate Program in Environmental Sciences, Av. Dr. Manuel Nava 201, Zona Universitaria, 78210, San Luis Potosi, SLP, Mexico*

[c]*Faculty of Chemical Sciences, Autonomous University of San Luis Potosi, Av. Dr. Manuel Nava No.6, Zona Universitaria, 78210. San Luis Potosi, SLP, Mexico.*

[d]*Universidade Federal de Santa Maria, Av. Roraima nº 1000, Cidade Universitária Bairro Camobi, Santa Maria – RS, CEP: 97105-900. Brasil.*

[e]*Coordination for Innovation and Application of Science and Technology, Av. Sierra Leona #550, Lomas 2a. Sección, 78210, San Luis Potosi, SLP, Mexico.*

[f]*Technological University of Izucar de Matamoros. De Reforma 168, Campestre la Paz, 74420, Izucar de Matamoros, Puebla. Mexico.*

[g]*National Polytechnic Institute, Blvd. del Bote 202, Cerro del Gato Ejido La Escondida, Ciudad Administrativa, 98160, Zacatecas, Mexico.*

[h]*Grupo de Investigacion en Materiales de Carbon/Dpto. Química Inorgánica/Universidad de Granada, Granada, Spain.*

[i]*Desert Zones Research Institute, Altair No. 200, Col. del Llano, 78377, San Luis Potosí, SLP. Mexico.*

***Corresponding Author:** nahum.medellin@uaslp.mx

Abstract

This work studied the application of adsorption with activated carbons (ACs) and photodegradation to reduce the concentration of triclosan (TCS) in aqueous solutions. Concerning the adsorption, the ACs (Darco, Norit, and F400) were characterized in detail, and batch experiments were applied to elucidate the effect of pH on the equilibrium. The results showed that at pH = 7, the maximum adsorption capacity of TCS onto the ACs was obtained, which was 18.5 mg g^{-1} for Darco, 16.0 for Norit, and 15.5 for F400. The Diffusional kinetic model allowed an adequate interpretation of the experimental data. The effective diffusivity varied and increased along with the amount of TCS adsorbed, from 1.06 to 1.68×10^{-8} cm^2 s^{-1}. In the case of photodegradation, the removal percentage of TCS and sulfate radicals were verified. It was possible to ensure that the triclosan molecule was sensitive to UV light of 254 nm since the removal was over 80 % using UV light. The removal of TCS was increased in the presence of sulfate radicals. It was possible to identify 2,4-dichlorophenol as one of the photolytic degradation products of triclosan, and it does not represent an environmental hazard at low concentrations of triclosan in water. These results confirm that the wastewater treatment methods proposed are effective for removing TCS from water, reaching levels of concentration that do not constitute a risk to human health or environmental hazard. Both methods effectively eliminate the pollutant with relatively easy techniques to implement.

Keywords: Triclosan; activated carbons; photodegradation; adsorption; emerging pollutants; radicals.

1. Introduction

The contamination of bodies of water by organic compounds is one of the leading environmental problems. Industries such as mining, metal smelting, fuel, and energy production from oil, fertilizers, and pesticides and their applications, among others, produce residues containing organic chemical species, which are transferred to the aquatic environment due to incorrect treatment or final disposal. When organic compounds appear in different ecosystems at concentrations above permissible levels, they can cause significant toxic effects on cells, human and environmental health. Furthermore, these pollutants can be bioaccumulated and biomagnified along the trophic chain, depending on the specific conditions and characteristics of the water source, bringing serious environmental consequences for the marine ecosystem and human health (Rainbow 1995, 2006; Moore and Ramamoorthy 2012). Among the wide range of pollutants, the study of the so-called emerging pollutants has prompted special interest in recent years. These contaminants have existed for decades, but only recently have they received much of the attention of the international scientific community. Moreover, these pollutants are unregulated in most countries and partially removed by most of the water treatment techniques implemented today (Singer et al. 2002).

Emerging pollutants are classified into different categories: microplastics, fertilizers, personal hygiene products, illegal drugs, antibiotics, and others. Personal and household hygiene products are commonly used and continuously discharged into the environment. Their active principles are concentrated and accumulated in specific matrices to the point of being already considered a contamination problem. TCS effectively eliminates bacteria, fungi, and protozoa, and it has antiseptic, preservative, and disinfectant properties. It is used as an additive in many consumer products (household cleaning products, cosmetics, toys,

plastics and paints, and others. (Singer et al. 2002). It is widely used in health devices, textile fibers, plastics, and kitchen utensils, in which it acts as a bactericide with long duration times (MØRETRØ et al. 2006). TCS is a potential endocrine disruptor (Allmyr et al. 2006a; Franz et al. 2008), altering thyroid hormone homeostasis (Allmyr et al. 2006b) and estrogen-dependent responses (Calafat et al. 2007).

Adsorption processes efficiently remove organic contaminants such as TCS from water (Behera et al. 2010). However, the scientific literature does not report many studies that prove it. The most relevant results show removal percentages higher than 80% when materials of carbonaceous origin are used (Behera et al. 2010). Therefore, it is important to develop and implement better technologies that minimize the negative impacts of TCS on the aquatic environment and human health. Activated carbons can play an important role in removing pharmaceutical compounds from the pharmaceutical industry, assuming that the concentration levels and physicochemical properties are similar to the reported for pesticides (Mohanty et al. 2006; Kazner 2011). In this sense, the adsorption capacity of biochars derived from different materials is currently studied, resulting in high removal percentages of TCS (Wang and Wang 2019; Cho et al. 2021).

Although adsorption is a widely used pollutant removal technique that allows considerable removal levels, in the case of organic pollutants with aromatic rings and photosensitive, removal techniques that include the principles of photo-oxidation are preferred, for which, in this work, the use of photolysis of TCS with ultraviolet light and radicals is proposed to evaluate the feasibility of this treatment and compare its results with those obtained with adsorption (Son et al. 2010). It has been reported the use of an integrated photosensitizing/adsorbent material for the removal of TCS from water (Marazuela and García-Fresnadillo 2020)

Photolysis is a chemical process whereby the absorption of light allows the breakdown of a molecule into smaller components. Light provides the energy required to break a molecule into its parts. These processes are also known as photodecomposition or photodissociation (Lemaire et al. 1982). Photolysis is an effective method to assist the existing treatment of sewage treatment plants with triclosan. However, there is the drawback that harmful dioxin and phenol-type intermediates (Mezcua et al. 2004) can be produced in the presence or not of chloride anions since there is a similarity between TCS and dioxin-derived compounds (Son et al. 2007).

Thus, the present work aims to evaluate the remotion capacity of ACs (Darco, Norit, and F400) to remove triclosan in an aqueous solution. Another objective is to study the general adsorption rate of triclosan and the mass transfer mechanism that determines it, using a diffusional kinetic model. The third objective is to analyze the efficiency of direct photodegradation and sulfate radicals in removing triclosan in an aqueous solution through comparative studies of concentrations at equilibrium. This information will be possible to compare these wastewater treatment methods to recognize their advantages and disadvantages and propose them as an alternative for the disinfection of polluted waters.

2. Experimental Methodology

2.1. Chemicals

The triclosan stock solution was prepared as reported by González-Fernández et al. (González-Fernández et al. 2021). After adsorption, the TCS concentration was determined

130 in a Genesys 10 S UV-Vis Spectrometer. The concentration of TCS in aqueous solution, after
131 photodegradation, was determined by a Reverse-Phase High-Performance Liquid
132 Chromatography (RP-HPLC) method similar to that reported by Medellín-Castillo et al.
133 (Medellin-Castillo et al. 2013). The chromatographic column was Agilent Technologies®
134 C_{18} (4.6x100 mm particle size, 3.5 µm).
135
136 *2.2. Activated carbons*
137
138 The commercial activated carbons Darco (Sigma Aldrich), Norit (Sigma Aldrich),
139 and F400 (Calgon Carbon Corporation) were used for the adsorption experiments. The ACs
140 were pre-treated as described by Segovia-Sandoval et al. (Segovia-Sandoval et al. 2019).
141 A porosimeter analyzer (Micromeritics, ASAP 2020) was used to determine the N_2
142 adsorption-desorption isotherms on ACs to evaluate the specific area (S_{BET}), pore volume
143 (V_p), average pore diameter (d_p), and other textural properties. In addition, the pore size
144 distribution was evaluated with the DFT method, and the BET method was used to determine
145 the specific area of the ACs.
146 The pH at the point of zero charge (PZC) was evaluated using an acid-based titration
147 method proposed by Babic et al. (Fiol and Villaescusa 2009), and the Boehm method (Boehm
148 1994) was used to determine the active sites concentration of ACs. The material morphology
149 was examined using a Scanning Electron Microscope (Quanta 250 FEG with Oxford brand
150 EDS probe).
151

152 *2.3. Adsorption isotherm experiments and calculations*

153

154 Triclosan stock solutions and sample solutions are prepared as described by
155 González-Fernández (González-Fernández et al. 2021). Then, the solution was transferred to
156 the batch adsorber and was left in contact with the AC until equilibrium. Finally, the global
157 mass balance equation calculated the adsorption capacity (q) of the ACs for TCS:

158

159 $$q = \frac{V_0 C_0 - V_f C_f - \sum_{i=1}^{N} V_i C_i}{m} \quad (1)$$

160 C (mg L^{-1}) and V (L) are the TCS concentration and solution volume. The subscripts *0* and *f*
161 are relative to the initial and final moments. The term Σ is relative to the sampling used for
162 quantification (mg), and m is the adsorbent amount (g)

163 The Langmuir (Langmuir 1918), Freundlich (Freundlich 1906), and Radke-Prausnitz
164 (Radke and Prausnitz 1972) adsorption isotherms were used to fit the data. The following
165 equations that relate the amount of TCS on the solid (q_e, mg g^{-1}) and the TCS concentration
166 in the liquid (C_e, mg L^{-1}) at the equilibrium condition, respectively, mathematically represent
167 these models:

168 $$q_e = \frac{q_m K_L C_e}{1 + K_L C_e} \quad (2)$$

169 $$q_e = K_F C_e^{1/n} \quad (3)$$

170 $$q_e = \frac{K_R C_e}{1 + a_R C_e^{1-\beta}} \quad (4)$$

171 Where: q_m is the maximum adsorption capacity (mg g^{-1}), K_L is the Langmuir constant (L mg^{-1}),
172 *1/n* is the exponent of the Freundlich model, K_F is the Freundlich constant (mg L^{-1})(mg g^{-1})$^{-1/n}$,
173 K_R (L g^{-1}), a_R (L mg^{-1}) and β are the R-P constants.

The Rosenbrock and *quasi*-Newton algorithms were used to estimate the adsorption isotherms parameters. The selection of the better fit among the isotherm models was made using the average percentage deviation ($\%D$) and coefficient of determination (R^2) described by the following equations:

$$\%D = 100 \cdot \frac{1}{k} \sum_{i=1}^{k} \frac{q_{ei,exp} - q_{ei,cal}}{q_{ei,exp}} \quad (5)$$

$$R^2 = 1 - \frac{\sum_{i=1}^{k} \left(q_{ei,exp} - q_{ei,cal}\right)^2}{\sum_{i=1}^{k} \left(q_{ei,exp} - \bar{q}_{ei,cal}\right)^2} \quad (6)$$

Where: k is the number of experimental points $q_{ei,exp}$ is the experimental adsorption capacity in each point (mg g^{-1}), $q_{ei,cal}$ is the predicted adsorption capacity in each point (mg g^{-1}) and $\bar{q}_{ei,cal}$ is the average of all estimated adsorption capacity values (mg g^{-1}).

2.4. Adsorption kinetic experiments

The kinetic decay curves were constructed at initial TCS concentrations of 10 and 15 mg L^{-1} and pH = 7. In these experiments, ACs were added and placed in the adsorber at 25 ºC. In addition, 2.0 mL samples were taken at selected time intervals, and their absorbance at 280 nm was measured in the UV-Vis spectrometer. Each experiment was performed in triplicate.

A Diffusional model (Pauletto et al. 2020, 2021; Moreno-Pérez et al. 2021) was used to describe the kinetic experiments, and the equations of this model were solved numerically by the COMSOL MULTIPHISICS using the “Mathematics” module. Details of the model are presented in section 3.6.

2.5. Photodegradation of TCS

A photoreactor equipped with a low-pressure mercury lamp was used to carry out UV degradation of TCS. This tube emitted ultraviolet light at a wavelength of 254 nm. Atrazine (ATZ) was used as an actinometric substance to evaluate the intensity of the irradiation of the lamp (Medellin-Castillo et al. 2013).

The photodegradation rate data was obtained by adding 50 mL of a TCS solution (ratio 1:5 Acetonitrile-H_2O mixture) into the reaction tube and was continuously mixed with a magnetic stirrer. The initial concentration of TCS in the solution was fixed between 10 and 60 mg L^{-1} at a constant temperature of 25 ºC. The reactor solution was sampled at the times of 1, 5, 10, 15, 20, 30 min, and the sample volume was 1.0 mL

The potassium persulfate solutions were added along with the TCS solution to the reaction tube to perform the radical photodegradation experiments. The concentration of potassium persulfate was varied between 0.5 and 5.0 mmol L^{-1}. The rest of the experimental conditions remained unchanged.

2.6. 2,4-Dichlorophenol Test Method

The concentration of 2,4-DCP was determined at the same wavelength as TCS and using the same experimental conditions already described. In brief, a solution of the compound was previously injected into the column at different concentrations, and its calibration curve was performed to achieve its quantification. It was also used Gas Chromatography coupled to a Mass Spectrometer (GC/MS) to identify this possible by-product.

3. Results and Discussions

3.1. Textural characterization of the ACs by N_2 physisorption

The textural properties of the three materials studied are shown in Table 1. The specific areas and pore volumes of these ACs were reported by other authors (Son et al. 2007; Moreno-Pérez et al. 2021; Pauletto et al. 2021). For example, Segovia-Sandoval et al. (Segovia-Sandoval et al. 2019) reported specific areas of 627, 971, and 871 $m^2\ g^{-1}$ for the activated carbons Darco, Norit, and F400, respectively. These values were estimated for materials with 20-40 mesh particle sizes. As can be seen, these values are close to those obtained in this work.

Table 1. Textural properties of adsorbents.

AC	S_{BET} ($m^2\ g^{-1}$)	V_{meso} (BJH) ($cm^3\ g^{-1}$)	$V_{0.95}$ ($cm^3\ g^{-1}$)	W_0 (N_2) ($cm^3\ g^{-1}$)	L_0 (N_2) (nm)
NORIT	943	0.089	0.491	0.331	1.14
F400	756	0.066	0.360	0.317	1.27
DARCO	651	0.504	0.593	0.285	1.83

The adsorption-desorption isotherms of nitrogen on the ACs are shown in Figure 1. The isotherms of Norit and F-400 carbons are type Ib (IUPAC classification) (Zdravkov et al. 2007). The Darco carbon isotherm is type IVa (IUPAC Classification) (Zdravkov et al. 2007). The type IVa isotherm has a hysteresis loop associated with the capillary condensation characteristic of adsorption/desorption in mesopores and a limit value in the amount adsorbed for the upper range of relative pressure. The hysteresis cycle type is H2 because the filling process of the mesopores is governed by the capillary condensation phenomenon and by the percolative properties of the solid (Hong et al. 2019).

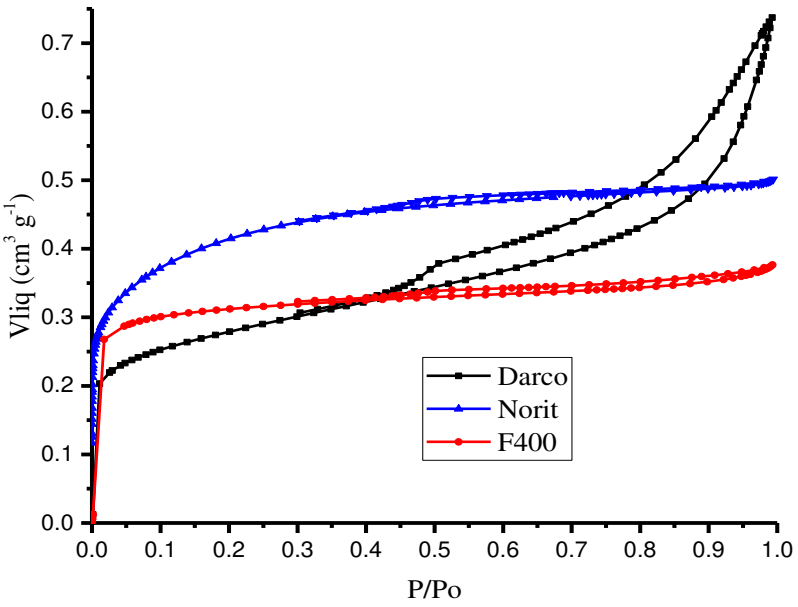

Figure 1. Adsorption-desorption isotherms of N_2 on ACs at 77K.

In the case of Darco AC, previous studies by Maffei et al. (Maffei et al. 2006) and Xu et al. (Xu et al. 2020) reported a type IVa isotherm for 20-40 and 100 mesh, respectively. In these studies, hysteresis loops of type H2 were observed at values of P/P_0 higher than 0.4. Citraningrum et al. (Citraningrum et al. 2007) investigated the adsorption-desorption of N_2 on Norit AC and found a similar behavior observed in this work. For the case of F400 AC, Carrales-Alvarado et al. (Carrales-Alvarado et al. 2016) and Segovia-Sandoval et al. (Segovia-Sandoval et al. 2019) reported similar results to those presented in this study and observed type Ib isotherm for this AC, typical of microporous materials where there is no capillary condensation in the pore system. The pore size distribution of the ACs is shown in Figure 2. As seen in this figure, Norit and F400 carbons are essentially microporous materials, while Darco AC has significant mesoporosity, so that the Darco AC had a hysteresis loop.

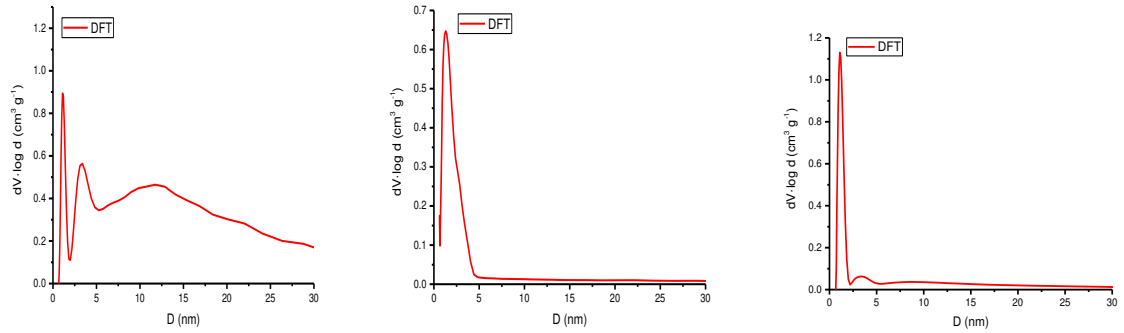

a) b) c)

Figure 2. Pore size distribution in adsorbent materials: a) Darco, b) Norit, c) F400.

3.2. Chemical characterization of ACs

Table 2 shows the concentrations of the active sites in the ACs. The concentrations of acid and basic sites agree with those reported for these activated carbons by Segovia-Sandoval et al. (Segovia-Sandoval et al. 2019).

Table 2. The concentration of active sites of the adsorbent materials and PZC.

Material	Acid (mmol g^{-1})				Basic (mmol g^{-1})	PZC
	Phenolic	Carboxylic	Lactonic	Total		
F400	0.092	0.068	0.008	0.168	0.308	8.25
NORIT	0.031	N/D*	0.098	0.129	0.278	8.75
DARCO	0.068	0.132	0.114	0.314	N/D*	6.00

***N/D: Non-Detected**

For the Darco AC, Xu et al. (Xu et al. 2020) could not detect basic sites in this AC. The Norit AC has a higher concentration of basic sites than acids. A similar result was also found by Carrott et al. (Carrott et al. 2001), reporting concentrations of acid and basic sites of 0.133 and 0.254 mmol g^{-1}. On the other hand, Rivera-Utrilla & Sánchez-Polo (Rivera-Utrilla and Sánchez-Polo 2002) reported a concentration of acid groups of 0.139 mmol g^{-1} for DARCO AC, which is close to that obtained in this work. For the F400 AC, the

concentration of basic sites is also higher than the acid sites, which coincides with that reported by Sotiropoulou et al. (Sotiropoulou et al. 2019), determining the total acidic and basic values of 0.116 and 0.117 mmol g^{-1}, respectively.

The discrepancies and similarities observed in the properties of ACs can be explained considering that the concentrations of the functional groups of an AC are essentially due to the manufacturing and activation process of the ACs. Besides, the AC surface can be enriched in one or other groups depending on the treatment carried out or the groups of the precursor material (Carrott et al. 2001; Rivera-Utrilla and Sánchez-Polo 2002; Sotiropoulou et al. 2019).

The PZC values of the ACs are shown in Table 2. The PZC of Darco AC is 6.0, indicating that its surface nature is acid, and that the concentration of basic sites is lower than that of acid sites, which agrees with the results described above. The PZC for this AC ranged from 4.25 (El-Sayed and Bandosz 2004) to 6.7 (Son et al. 2007) in the technical literature. The PZC of Norit AC is 8.75, revealing that it is a basic adsorbent, and the PZC for this AC was determined in previous works and varied considerably from 2.2 to 11.8 (Lopez-Ramon et al. 1999; Rivera-Utrilla and Sánchez-Polo 2002; Perez-Cadenas et al. 2003; El-Sayed and Bandosz 2004; Wang et al. 2007; Medellin-Castillo et al. 2013; Sotiropoulou et al. 2019).

3.3. Scanning Electron Microscopy with Energy Dispersive X-rays (SEM/EDX) Analysis

The AC surface morphology was analyzed in a scanning electron microscope, and the images of the ACs at 5000 kx are depicted in Figure 3.

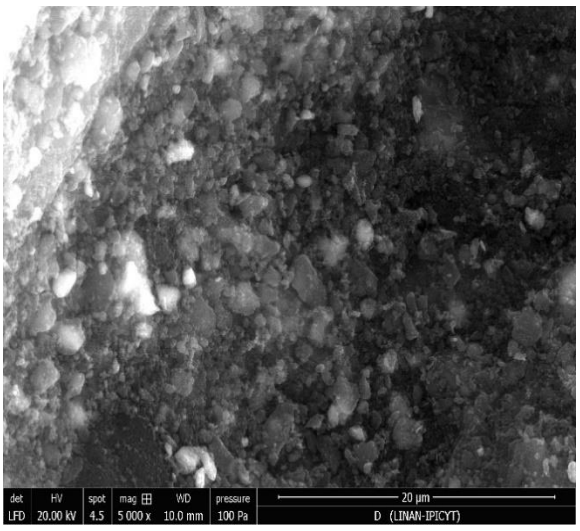

a)

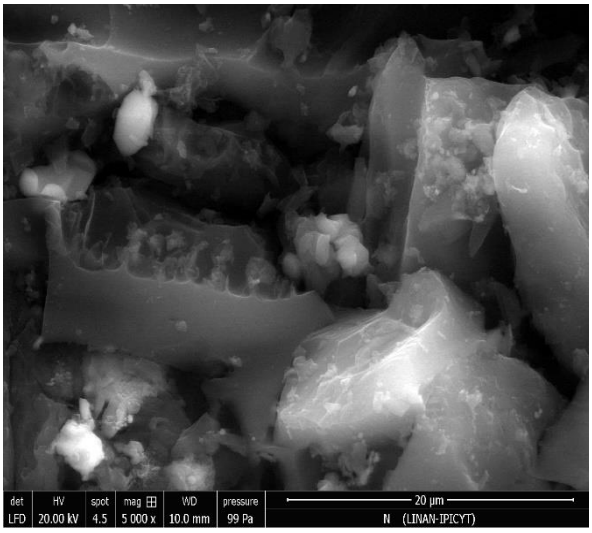

b)

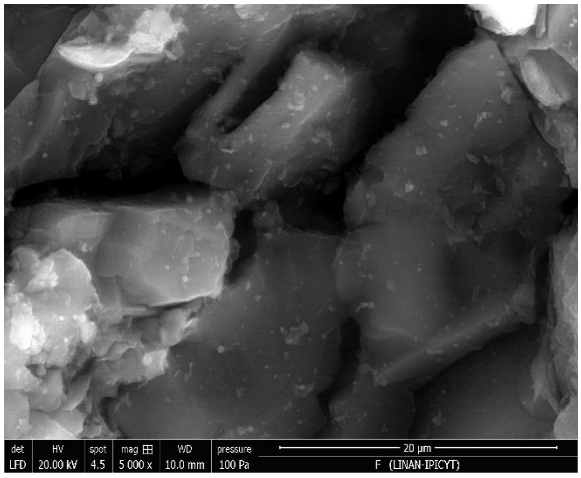

c)

Figure 3. Photomicrographs of the adsorbent materials: a) Darco, b) Norit, and c) F400.

All ACs show similar surface morphologies, and many cavities and channels were observed. A marked effect of AC porosity, where tunnels were observed, favored the pollutant diffusion in the adsorbent materials. Besides, Norit and F400 ACs exhibited fractured, rough, and porous surfaces. It is also noticed that the shapes and sizes of the particles of these ACs are very irregular. In addition, the particle size distribution is not uniform.

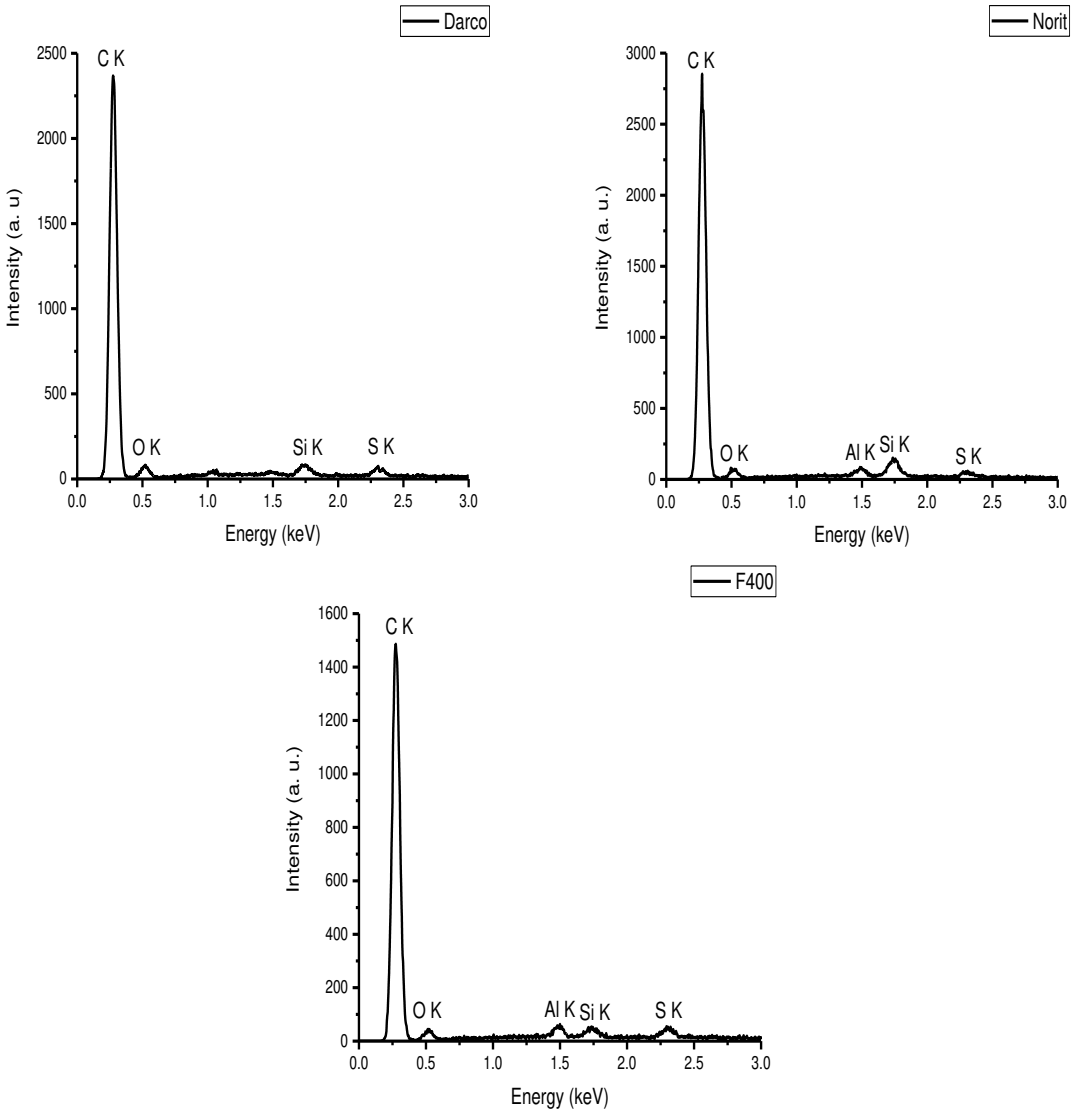

Figure 4. X-ray dispersive energy spectrum corresponding to a point analysis on the particle surface of adsorbents.

Figure 4 shows the EDS microanalysis at a point on the AC surface. In this figure, it can be seen that the activated carbons are composed of the elements C, O, Si, S, and Al. This result is due to the impurities of catalysts and chemical reagents used during the activation process of commercial activated carbons (Lopez-Ramon et al. 1999; Perez-Cadenas et al. 2003; El-Sayed and Bandosz 2004; Wang et al. 2007).

306 *3.4. Triclosan adsorption isotherms on ACs*

307

308 The adsorption isotherms of TCS on the adsorbents at 25 ºC and three pH values are
309 shown in Figure 5. The mathematical equations of the Radke-Prausnitz, Freundlich, and
310 Langmuir isotherms were selected to explain the experimental data. Using the Rosenbrock-
311 Newton algorithm, the adsorption isotherm parameters of Freundlich, Langmuir and Radke-
312 Prausnitz were evaluated and are listed in Table 3. According to a criterion of lower
313 percentage deviation and higher coefficient of determination, it was found that the Radke-
314 Prausnitz isotherm interpreted the data better in all cases. So, the lines in Figure 5 were drawn
315 using this model.

316 The Radke-Prausnitz isotherm adequately describes the experimental adsorption
317 equilibrium data in some adsorbate-adsorbent systems. In addition, this isotherm reveals that
318 the ACs have both homogeneous and heterogeneous sites (energetically) for TCS adsorption,
319 and this behavior has been previously reported (Babić et al. 1999).

320

321

322

323 **Table 3.** Parameters of the isotherms for the adsorption of TCS on the ACs.

324

AC	pH	Langmuir				Freundlich				Radke-Prausnitz				
		q_m (mg g^{-1})	K_L (L mg^{-1})	%D	R^2	K_F (mg g^{-1})(L mg^{-1})$^{-1/n}$	n	%D	R^2	K_R (L g^{-1})	a_R (L mg^{-1})	1-β	%D	R^2
Darco	7	24.36	0.70	9.62	0.9957	9.65	2.20	18.02	0.8955	11.63	0.16	1.65	2.06	0.9990
	10	21.05	0.49	16.82	0.8949	7.43	2.49	25.37	0.9121	5.61	0.01	2.49	5.97	0.9968
	11	18.87	0.47	5.26	0.9840	6.37	2.34	9.65	0.9671	12.27	0.97	0.83	5.94	0.9860
Norit	7	19.71	0.70	5.18	0.9657	8.20	2.66	15.49	0.8815	8.73	0.17	1.46	6.89	0.9851
	10	19.07	0.49	17.94	0.8753	6.93	2.63	25.99	0.7464	5.22	0.02	2.10	5.97	0.9697
	11	15.31	0.66	6.92	0.9616	6.56	3.09	16.10	0.8381	6.86	0.22	1.31	2.69	0.9919
F400	7	18.46	0.64	4.04	0.9858	7.42	2.70	14.02	0.9081	8.68	0.27	1.25	3.76	0.9951
	10	13.30	0.63	3.95	0.9906	5.71	3.23	12.92	0.8925	6.82	0.37	1.13	1.81	0.9978
	11	15.54	0.15	8.11	0.9662	2.76	1.93	13.15	0.9101	1.53	0.005	2.09	0.64	0.9997

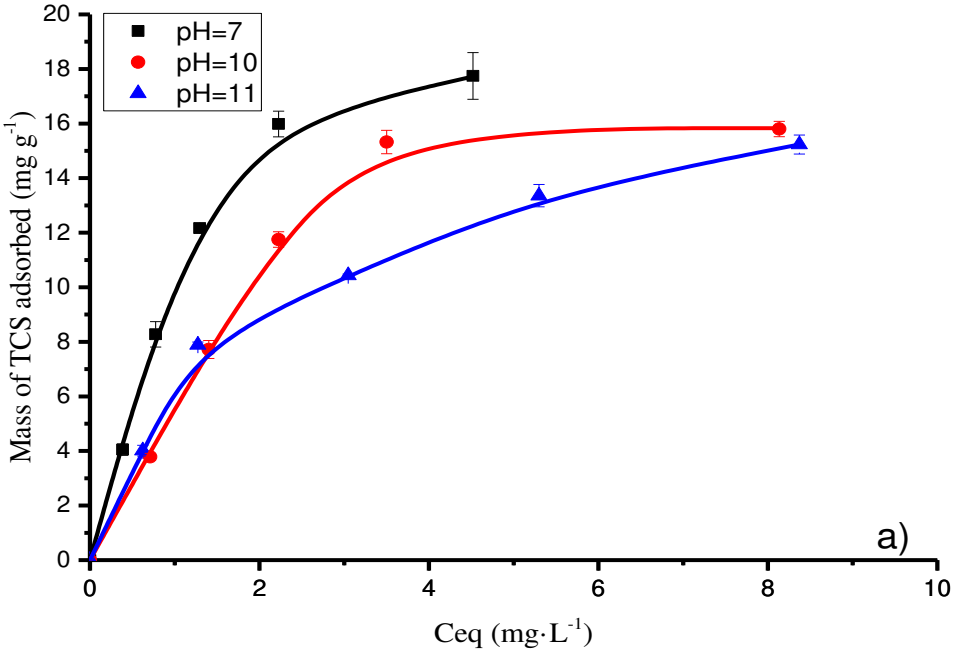
pH=7
pH=10
pH=11
Mass of TCS adsorbed (mg g-1)
Ceq (mg·L-1)
a)

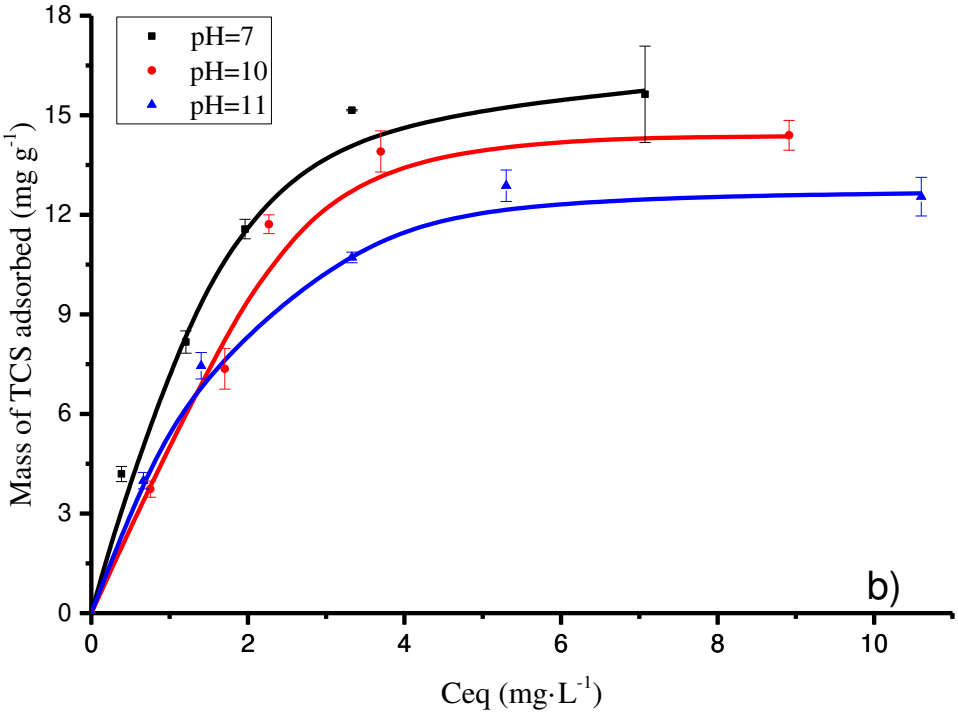
pH=7
pH=10
pH=11
Mass of TCS adsorbed (mg g-1)
Ceq (mg·L-1)
b)

325

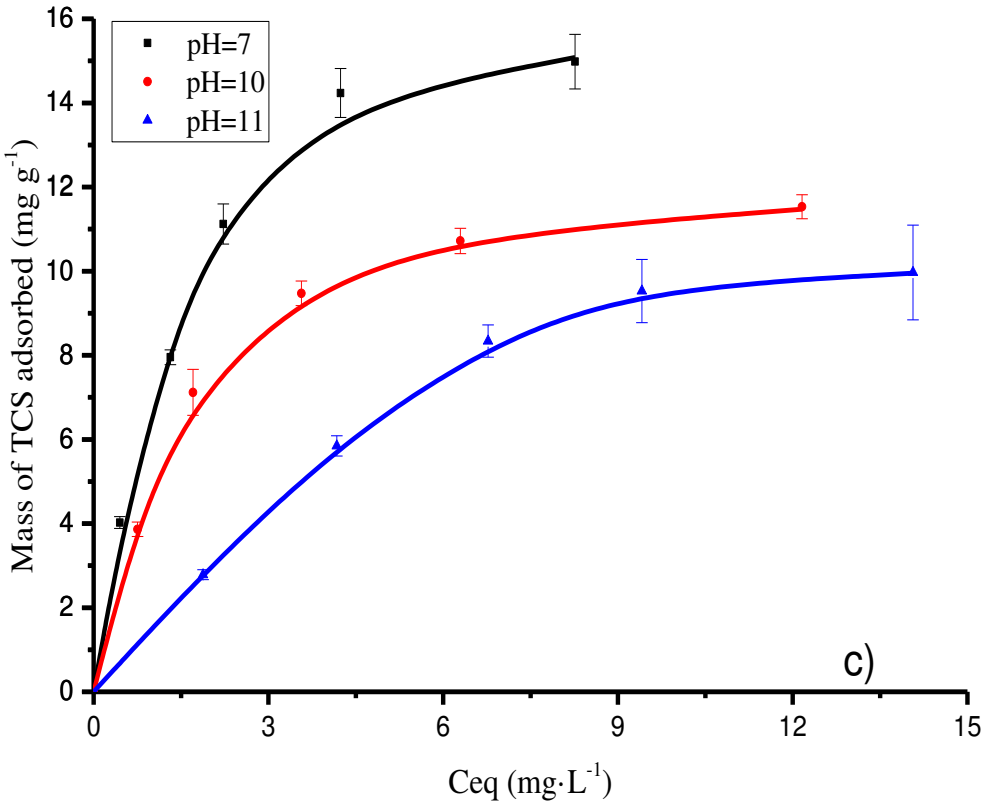

326

327 **Figure 5.** Adsorption isotherms of TCS on ACs: a) Darco, b) Norit, c) F400.

328

329 In Figure 5, it is observed that the isotherms show two stages. In the first stage, the
330 adsorption capacity increases by raising the triclosan concentration at equilibrium. This trend
331 is because the material initially has many active sites to retain triclosan from the solution. As
332 the concentration of triclosan increases, these sites become occupied, and it is more difficult
333 to find empty adsorption sites for adsorption. At this condition, a second stage is observed,
334 decreasing the slope of the adsorption isotherm until it reaches a saturation level, different
335 for each material. The maximum experimental adsorption capacity (q_m) is determined in this
336 second part of the isotherms.

337

338 *3.5. The effect of pH upon the adsorption capacity of ACs*

339

340 In the isotherms presented in Figure 5, it can be noticed that the mass of TCS adsorbed
341 is the highest at pH = 7, and the adsorption capacity decreases by increasing the pH. This
342 trend is because the neutral or undissociated species of TCS is predominant at the solution
343 pH less than pKa (Figure 6). In contrast, the anionic species of TCS is solely found at pH =
344 10 and pH = 11 (pH> pKa).

345 Changes in the pH modify the dissociation degree of the TCS molecule. At a pH value
346 above pKa (7.9), more than 50 % of the TCS in the solution is deprotonated. As a general
347 rule, when pH increases, the functional groups on the material´s surface are totally or partially
348 deprotonated, which leads to an accumulation of negative charges (Lopez-Ramon et al.
349 1999).

350 When pH > 7.9 (pKa), TCS is negatively charged, and the total charge on the surface
351 of the adsorbents has a negative sign when the adsorption occurs above the PZC. This trend
352 causes a reduction in the adsorption capacity due to the repulsion that occurs between the
353 charged TCS and the negative charges on the surface of the material. Conversely, when the
354 hydrogen ion concentration in the medium is high, the charge of the AC is positive, and the
355 TCS molecule is not dissolved, which minimizes repulsive interactions, increasing
356 adsorption. Authors like Babić et al. (Babić et al. 1999) have reported similar behavior.

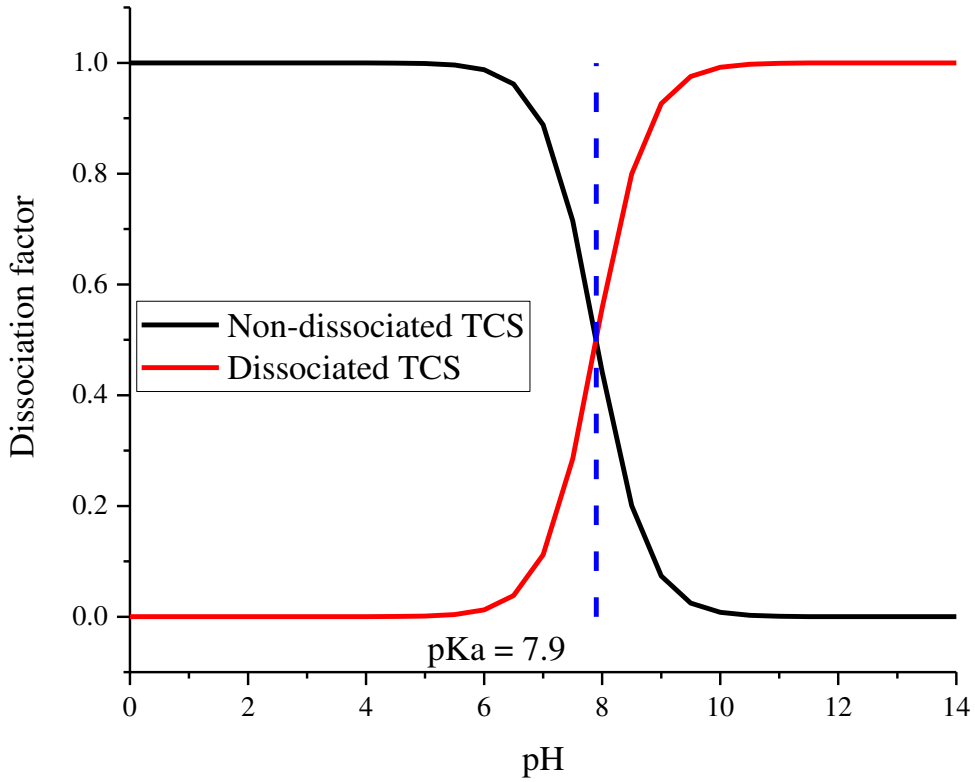

Figure 6. TCS species distribution diagram.

The higher adsorption capacity of Darco AC is because the Darco material has a porous lattice with a high contribution of mesopores. In this way, the adsorption of triclosan can be carried out with less steric effects than in Norit and F400 carbons, which are essentially microporous. Authors such as Andrade et al. (Andrade et al. 2018) corroborated this trend. In addition, Norit carbon has a higher area than F400 carbon, which can directly influence its adsorption capacity. Then, there is less surface available for adsorption on the F400 carbon, which means fewer active sites and less adsorption capacity in it.

367 *3.6. Diffusional model results*

368

369 The adsorption rate of TCS on ACs was interpreted by a diffusional model proposed
370 by Leyva-Ramos and Geankoplis (Leyva-Ramos and Geankoplis 1985). The following
371 equations represent the diffusional model considering the external mass transport and
372 intraparticle diffusion of the TCS during adsorption on AC:

373 $$V\frac{dC_A}{dt} = -mSk_L\left(C_A - C_{A,R}\right) \quad (7)$$

374 $$t = 0;\ C_A = C_{A0} \quad (7.a)$$

375 $$\varepsilon_p\left(\frac{\partial C_{A,r}}{\partial \mathrm{t}}\right) + \rho_p\frac{\partial \mathrm{q}}{\partial \mathrm{t}} = \frac{1}{r^2}\frac{\partial}{\partial \mathrm{r}}\left[r^2\left(D_{e,p}\frac{\partial C_{A,r}}{\partial \mathrm{r}}\right)\right] \quad (8)$$

376 $$C_{A,r} = 0; t = 0; 0 \le r \le R \quad (8.\ a)$$

377 $$\left.\frac{\partial C_{A,r}}{\partial \mathrm{r}}\right|_{r=0} = 0 \quad (8.\ b)$$

378 $$\left.D_{e,p}\frac{\partial C_{A,r}}{\partial \mathrm{r}}\right|_{r=R} = k_L\left(C_A - C_{A,R}\right) \quad (8.\ c)$$

379 $$q = f\left(C_{A,r}\right) \quad (9)$$

380 In this model, C_A (mg L^{-1}) is the TCS concentration in the liquid phase that varies with time
381 t (min or h), C_{A0} (mg L^{-1}) is the initial TCS concentration in the liquid phase, k_L (cm s^{-1}) is
382 the external mass transfer coefficient, $C_{A,\,R}$ (mg L^{-1}) is the TCS concentration at r=R, S (g
383 cm^{-2}) is the external surface area of the adsorbent, ε_p (-) is the particle porosity, $C_{A,r}$ (mg L^{-1})
384 is the TCS concentration inside the particle varying with time and position (r), ρ_p (-) is the
385 particle specific mass (g cm^{-3}) and $D_{e,p}$ is the intraparticle diffusivity (cm^2 s^{-1}).

386 The ordinary and partial differential equations presented above were solved
387 numerically by the COMSOL MULTIPHISICS. In this software, a dimension of one-

388 dimensional space was used, and in the physics of the problem, the "Mathematics" module
389 was used to solve the differential equations. The parameters and experimental conditions of
390 the model were loaded, and the parameter $D_{e,p}$ was optimized until the value that best
391 described the experimental data was found.

392 The interpretation of the experimental concentration decay curves by the diffusional
393 model is shown in Figure 7. The two mass transport parameters are the effective diffusivity,
394 $D_{e,p}$, and the external mass transport coefficient, k_L. The latter was estimated by the procedure
395 proposed by Furusawa & Smith (Furusawa and Smith 1973) and using Equation 6.

396 The estimated k_L values are shown in Table 4, and it is noted that they varied between
397 2.97×10^{-7} and 19.7×10^{-7} cm s^{-1} and are below the experimental k_L values obtained for the
398 adsorption rate of heavy metals and organic compounds on ACs (Furusawa and Smith 1973;
399 Leyva-Ramos and Geankoplis 1985). This result can be explained considering that, in this
400 adsorption rate study, the first concentration sample was taken at 1 h, and the value of k_L was
401 a rough estimate. Furthermore, the adsorption kinetics is very slow compared to other
402 systems, implying the importance of both external mass transfer and intraparticle diffusion.
403

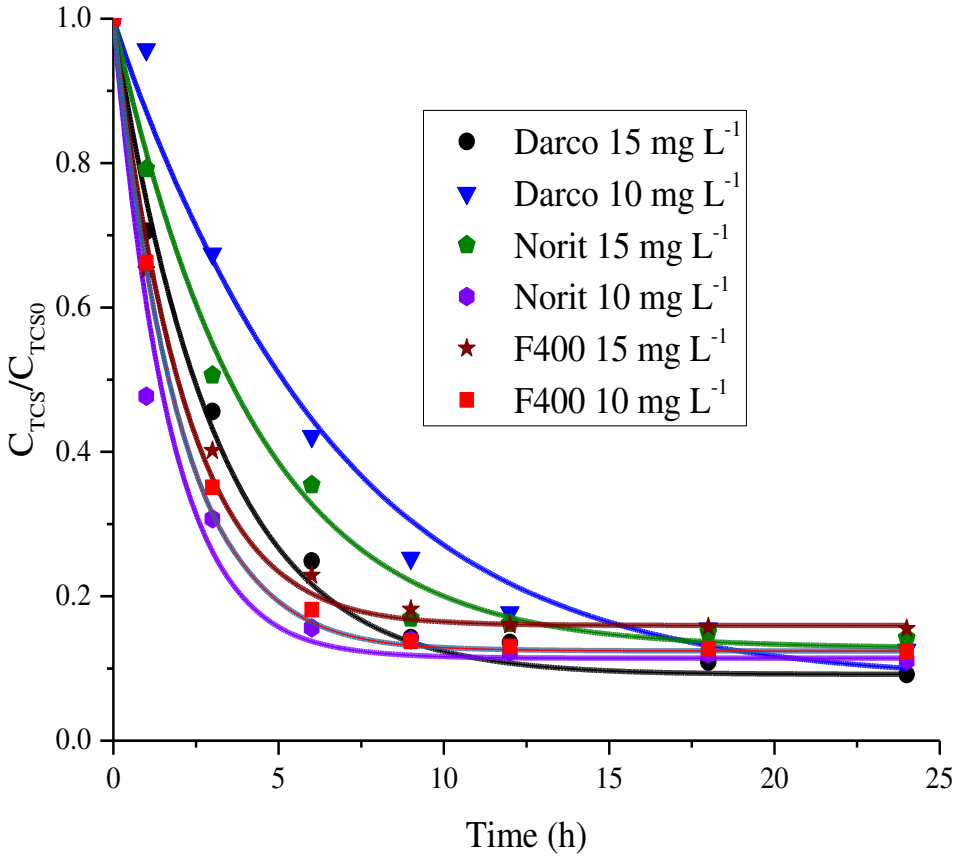

404 **Figure 7.** Decay curves of TCS concentration during adsorption on ACs. The lines represent
405 the predictions of the diffusional model.

406

407 The final equilibrium conditions were calculated by a mass balance of TCS at
408 equilibrium. This balance is expressed as follows:

409 $$VC_{A0} = VC_{Ae} + mq_e \quad (10)$$

The terms C_{Ae} and q_e were related by the Radke-Prausnitz adsorption isotherm. Therefore, the values of C_{Ae} and q_e were evaluated by simultaneously solving the equations of the adsorption isotherms and are shown in Table 4.

Table 4. Conditions of the experiments of the decay of TCS concentration in aqueous solution on the AC, equilibrium conditions, and mass transfer parameters at pH = 7 and 25 ºC.

AC	Exp. No.	C_{A0} (mg L^{-1})	m (g)	C_{Ae} (mg L^{-1})	$D_{e,p}\times10^6$ (cm^2 s^{-1})	q_e (mg g^{-1})	$k_L\times10^7$ (cm s^{-1})	ε	τ_p	R^2
Darco	**D15**	15.28	0.0517	1.40	1.10	10.20	6.14	0.55	4.6	0.9923
Darco	**D10**	10.02	0.0517	0.26	1.06	7.18	2.97	0.55	4.6	0.9915
Norit	**N15**	15.08	0.0517	2.90	1.64	8.95	4.43	0.54	3.1	0.9978
Norit	**N10**	10.06	0.0501	0.71	1.51	7.10	11.50	0.54	3.2	0.9965
F400	**F15**	15.06	0.0520	2.64	1.64	9.08	17.70	0.55	3.1	0.9925
F400	**F10**	10.08	0.0530	0.23	1.68	7.07	19.70	0.55	2.9	0.9947

Table 4 summarizes the effective diffusion coefficient ($D_{e,p}$) of TCS, the void fraction (ε) for the ACs, along the tortuosity (τ_p) values calculated. Tortuosity values vary between 2.9 and 4.6. In the case of ACs, several authors such as Leyva-Ramos et al. (Leyva-Ramos et al. 2007) and Ocampo-Pérez et al. (Ocampo-Pérez et al. 2012) reported tortuosity values around 2.5 and up to 6.5 for activated carbons. Besides, the *De,p* coefficient variations are not significant, and the experimental data was quite well described using the diffusional model (see R^2 in Table 4).

3.7. Photodegradation results

Figure 8 shows the decay curves of the triclosan concentration for different initial concentration values in an aqueous solution at a temperature of 25 °C.

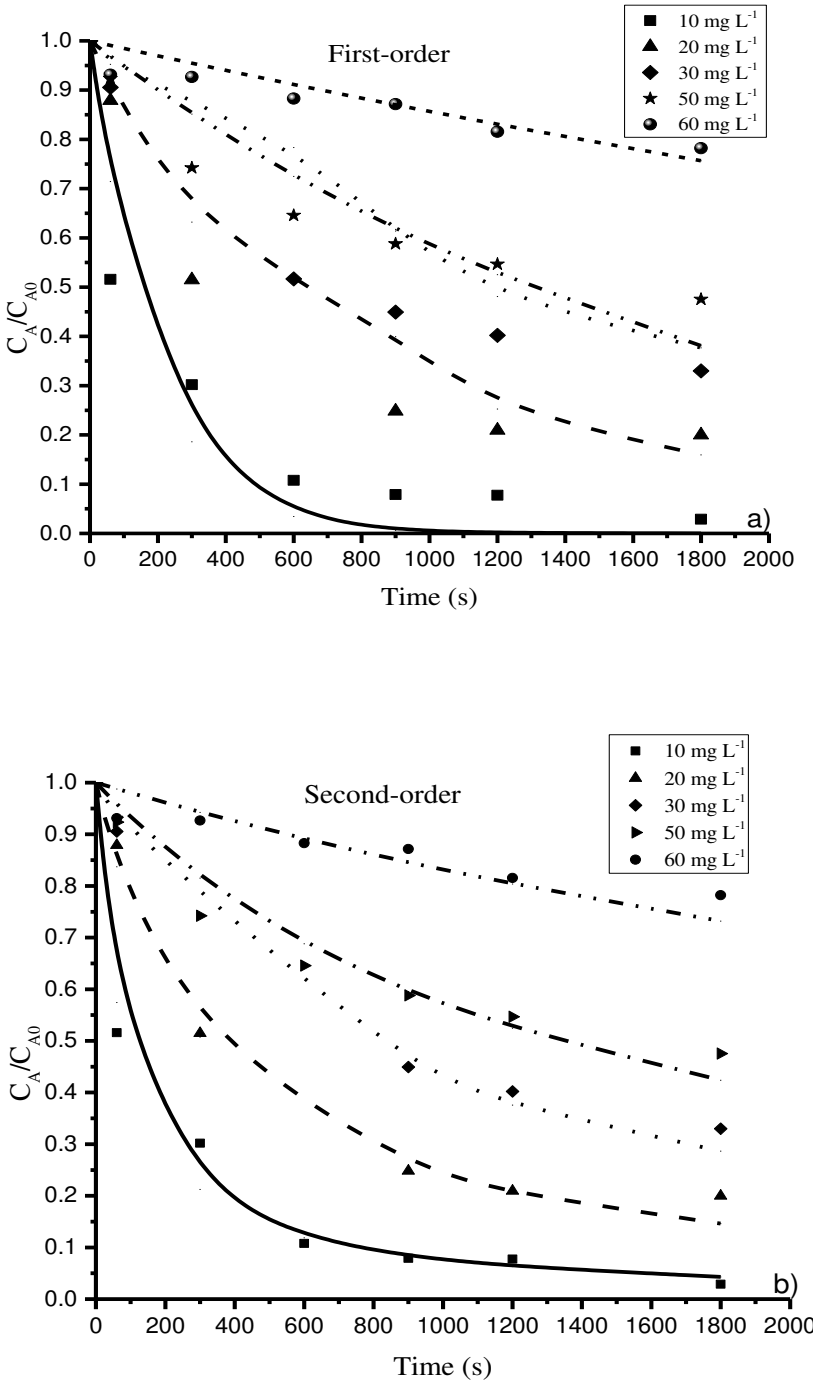

Figure 8. Effect of the initial concentration of TCS at 25 °C on photodegradation.

The data obtained in the experiment was interpreted with the following equations that represent the first and second-order models, respectively:

$$-\frac{dC_{TCS}}{dt} = k_{TCS1}C_{TCS} \quad (11)$$

$$-\frac{dC_{TCS}}{dt} = k_{TCS2}C_{TCS}^2 \quad (12)$$

Where: k_{TCS1} (s^{-1}) and k_{TCS2} (L mg^{-1} s^{-1}) are the first-order and second-order kinetic constants. Both constants were estimated using the Statistica Software®. The values of the constants k_{TCS1} and k_{TCS2}, as well as the determination coefficients, are shown in Table 5.

Table 5. Kinetic constants for photo-oxidation of TCS at 25 ºC.

C_{TCS}^0 (mg L^{-1})	$k_{TCS1} \times 10^6$ (s^{-1})	R^2	$k_{TCS2} \times 10^6$ (L mg^{-1} s^{-1})	R^2	Φ_{TCS} (mol $Einstein^{-1}$)
60	155	0.8165	2	0.9280	8.41×10^{-5}
50	536	0.8684	10	0.9554	4.21×10^{-4}
30	813	0.9417	44	0.9784	1.85×10^{-3}
20	1529	0.9431	146	0.9946	6.14×10^{-3}
10	5604	0.9058	1583	0.9843	6.67×10^{-2}

The second-order kinetic model adequately describes the results (R^2 > 0.90) in all cases). Besides, the curves predicted with de first-order kinetic model do not fit the experimental values for the TCS initial concentrations of 20, 30, and 40 mg L^{-1}. It can also be observed that both kinetic constants decrease with the increase in the initial concentration, a behavior also reported by Medellin-Castillo et al. (Medellin-Castillo et al. 2013) for the photodegradation of another organic compound.

446 The efficiency of ultraviolet light in photodegradation is related to quantum
447 efficiency. Therefore, the quantum yield of TCS (Φ_{TCS}) was evaluated with the following
448 equation (Medellin-Castillo et al. 2013):

449 $$\Phi_{TCS} = \Phi_{ATRZ} \frac{k_{TCS2}\varepsilon_{ATRZ}}{k_{ATRZ}\varepsilon_{TCS}} \quad (13)$$

450 Where: k_{TCS2} is the second-order photodegradation kinetic constant (L mg^{-1} s^{-1}), Φ_{ATRZ} is
451 0.046 mol $Einstein^{-1}$, ε_{ATRZ} is 386 m^2 mol^{-1} for λ = 254 nm (Hessler et al. 1993) and k_{ATRZ} is
452 1.82 x 10^{-3} s^{-1}.

453 The Φ_{TCS} values estimated with the previous equation ranged from 8.41×10^{-5} to
454 6.66×10^{-2} mol $Einstein^{-1}$. These results indicated that direct photodegradation was not very
455 efficient, and the photodegradation process becomes less efficient by increasing the
456 concentration of TCS. The efficiency of the process can be improved by adding small
457 amounts of potassium persulfate to the photoreactor solution.

458 Figure 9 shows the photodegradation kinetic curves of TCS in the UV/$S_2O_8^{2-}$ system
459 when the TCS concentration is close to 60 mg L^{-1}, pH = 7, and initial potassium persulfate
460 concentrations are 0.5, 1.0, 2.0, 5.0, and 10.0 mM, respectively.

461 The results in Figure 9 show that the TCS photodegradation rate was much faster
462 when potassium persulfate was added to the photo-oxidation system. For example, the k_{TCS2}
463 value is 30×10^{-6} L mg^{-1} s^{-1} for an initial potassium persulfate concentration of 0.5 mM,
464 whereas k_{TCS2} for direct photodegradation was 15 times slower. This improvement can be
465 attributed to the presence of sulfate and hydroxyl radicals, which catalyzed the breaking
466 down of TCS molecules into lower molecular by-products. The sulfate and hydroxyl radicals

467 were generated by the ultraviolet light decomposition of the potassium persulfate (Liang et
468 al. 2006).

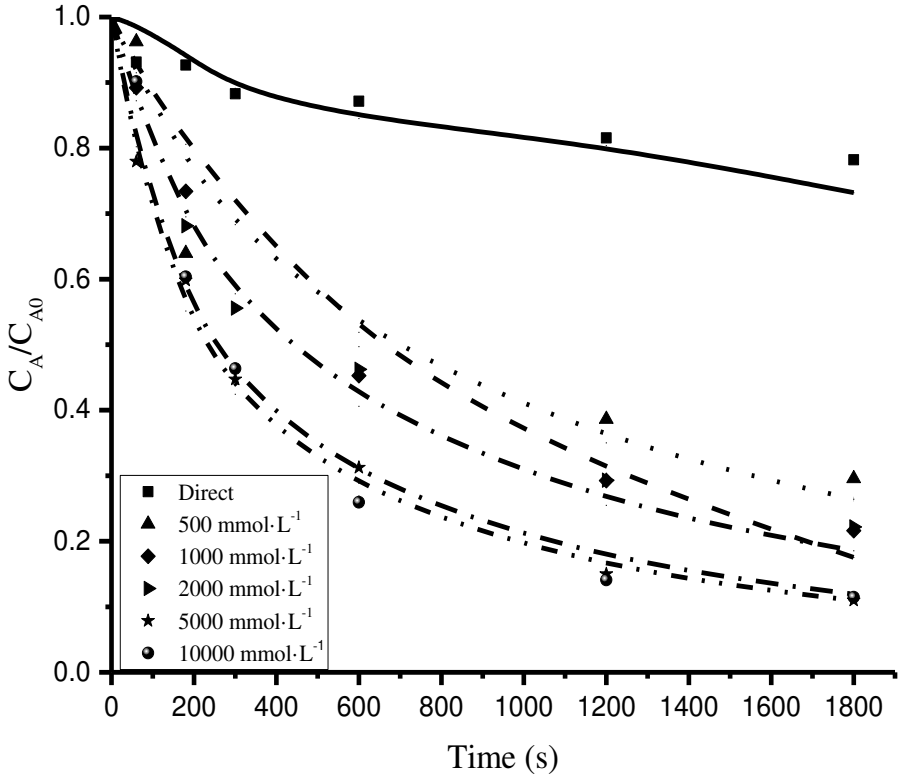

469

470 **Figure 9.** Effect of potassium persulfate concentration on the photodegradation of TCS at 25
471 ºC and TCS_0 = 60 mg L^{-1}. The lines represent the second-order kinetic model.

472

473 *3.8. Identification of photodegradation by-products*

474

475 The photodegradation of TCS in UV light leads to the breakdown of the molecule
476 into different degradation by-products. Several authors have reported that the
477 photodegradation mainly forms three by-products at an irradiation wavelength of 254 nm:
478 2,4-dichlorophenol, a quinone, and hydroquinone of TCS (Son et al. 2007, 2010).

During the photodegradation of TCS, three fundamental peaks could be observed in the chromatogram. Two of them are very close in retention time (between 1.8 and 2.2 min), and the third is close to 2.5 minutes. Two methods were used to identify 2,4-dichlorophenol, a recalcitrant compound and very harmful to the environment. The first one consisted of identifying it by obtaining its chromatogram and retention time on the column, keeping the same experimental conditions.

For this, the absorption spectrum in the UV region of 2,4-dichlorophenol was first obtained (Figure 10), with which it was possible to corroborate that it has an absorption maximum of around 280 nm. Therefore, it can be detected at the same wavelength as triclosan. Subsequently, a 2,4-dichlorophenol solution was analyzed in the HPLC equipment, and a retention time of 2.5 minutes was obtained. With this result, it was possible to define that the peak obtained at 2.5 min in the decomposition of triclosan corresponds to 2,4-dichlorophenol. Furthermore, it was possible to quantify this degradation by-product from this result.

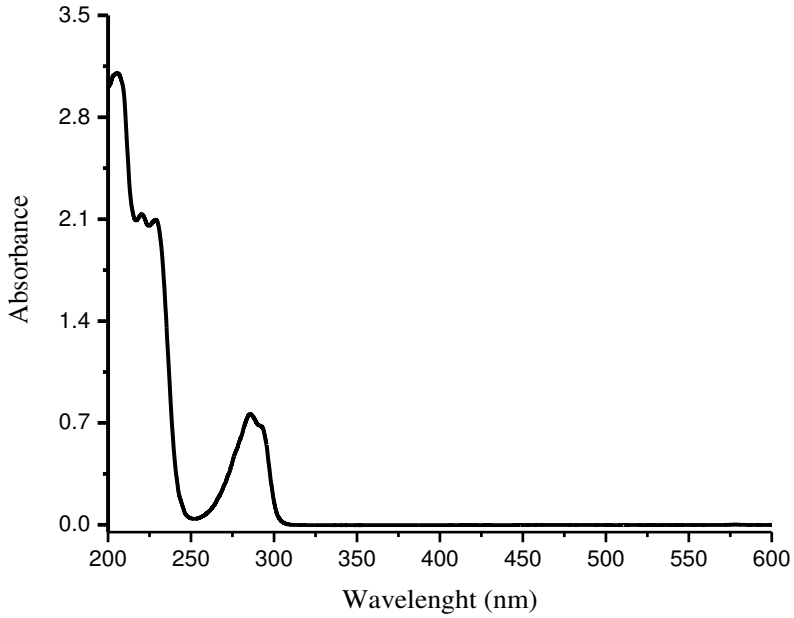

493

494 **Figure 10.** The ultraviolet absorption spectrum of 2,4-dichlorophenol.

495 As shown in Figure 11, at low values of triclosan concentration, 2,4-dichlorophenol
496 begins to form and then decreases its concentration. This trend is because its formation rate
497 is lower than its decomposition rate by UV light under these conditions (Latch et al. 2003;
498 Nfodzo and Choi 2011). However, when the concentration of triclosan increases, the by-
499 product formation rate increases, exceeding the decomposition rate, which is why sustained
500 growth is observed in the curve.

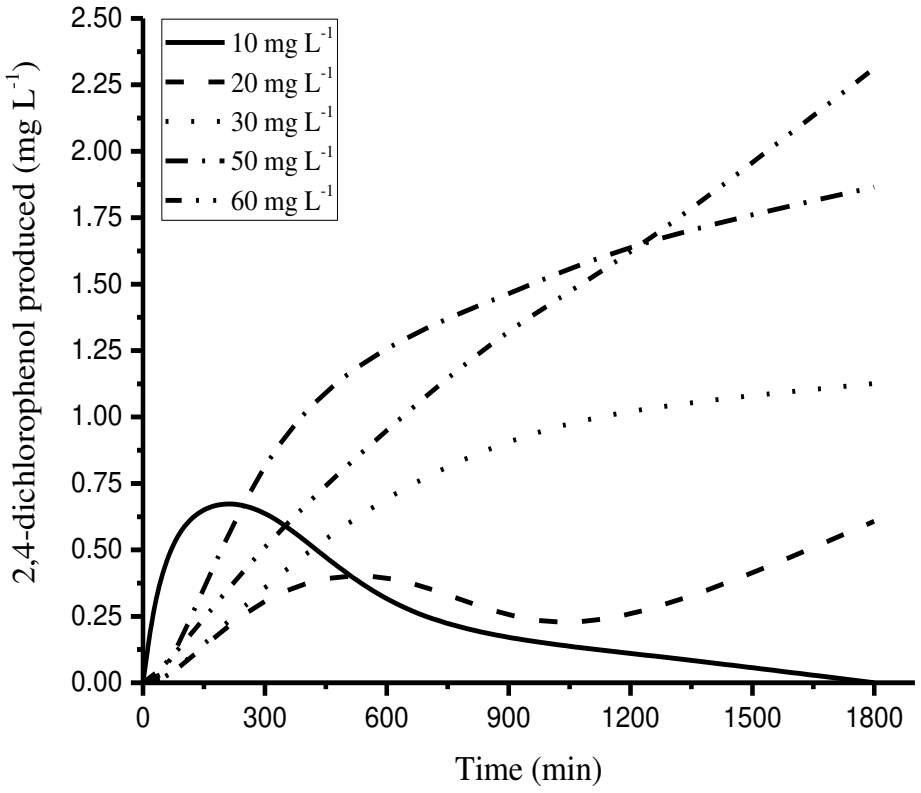

501

502 **Figure 11.** The concentration of 2,4-dichlorophenol as a by-product of direct photolysis of
503 triclosan at 254 nm.

504

505 This by-product obtained is a compound with a considerable negative environmental
506 impact, whose persistence and environmental effects are discussed by various authors
507 (Krijgsheld and Van der Gen 1986; Ensley et al. 1994).

508 The amount of 2,4-dichlorophenol formed represents a very low percentage in the
509 photolytic decomposition of triclosan, which does not represent an environmental problem.
510 It must also be considered that in wastewater, the concentration of triclosan does not, as a

general rule, exceed the order of nanograms per liter of solution, so the amount formed would be minimal compared to the amount of triclosan that would be removed.

The 60 mg L^{-1} of triclosan sample degraded with UV light for 30 minutes was analyzed in a Gas Chromatograph coupled to a Mass Spectrometry detector. The analysis resulted in the identification of triclosan and 2,4-dichlorophenol as degradation by-products of triclosan, in addition to other peaks that may correspond to the harmless quinone and hydroquinone by-products of triclosan (Son et al. 2007, 2010). The chromatogram obtained is shown in Figure 12.

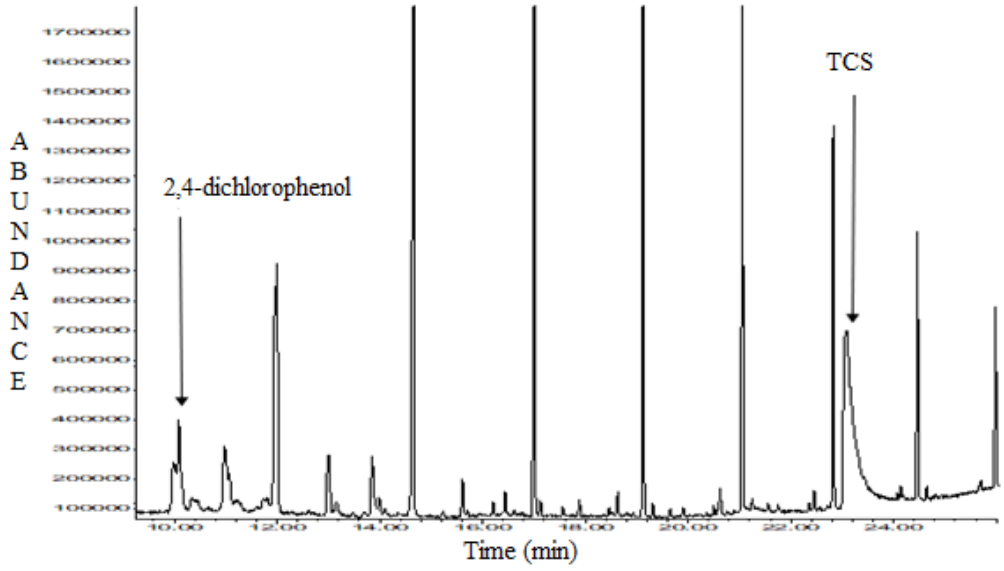

Figure 12. Chromatogram of the photolytic decomposition of TCS at 254 nm.

The triclosan and dichlorophenol compounds were identified through their mass spectra (Figure 13), which are shown below:

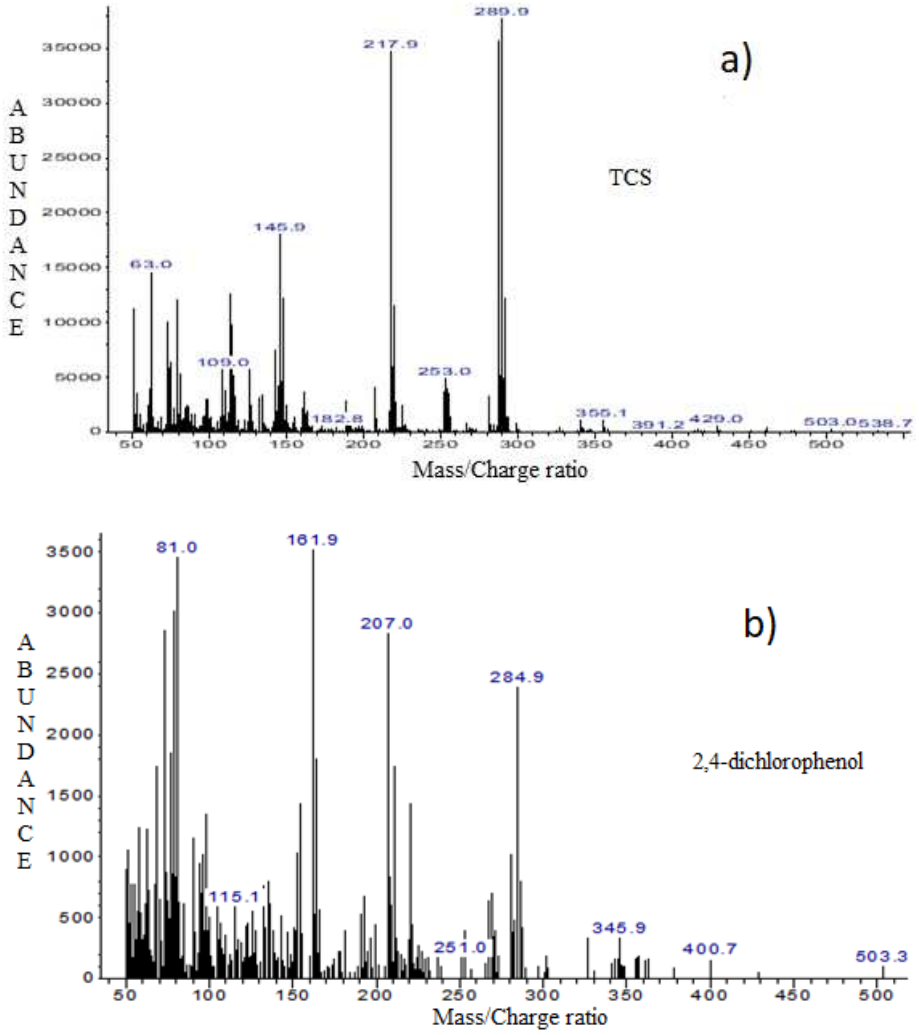

Figure 13. Mass spectra of a) triclosan, b) 2,4-dichlorophenol.

3.9. Pro-Cons Analysis of both techniques

This work allowed us to arrive at these results, which helped us make decisions regarding these technologies proposed for the elimination of triclosan from water. The results obtained in the experiments carried out allow us to corroborate that the wastewater treatment methods used effectively remove triclosan from the water and allow us to reach levels of its

concentration that do not constitute a risk to human or environmental health. Furthermore, both methods allow us to eliminate the pollutant with techniques that are relatively easy to implement, although their cost-benefit varies if the factors that determine them are analyzed.

The maximum removal percentage was reached with AC Darco at a pH value of 7, which was around 81 %. This percentage was achieved using 0.05 g of adsorbent and an initial concentration of TCS of 25 mg L^{-1}. In the case of photodegradation, the maximum removal efficiency without adding radicals and for a similar initial concentration value of the pollutant is of the order of 80 % using an initial concentration of 60 mg L^{-1}. These results indicate that both treatments are similarly efficient for eliminating TCS in an aqueous solution. The addition of radicals increases the degradation efficiency when the concentration of the pollutant in the solution is high. Therefore, it constitutes an alternative for remediation at high concentrations.

In the case of adsorption, it is a relatively expensive technique that allows us to eliminate triclosan from the water with commercial activated carbons that do not have a cheap cost. However, it allows removing the contaminant until obtaining very low levels of it in the remainder. Additionally, this technique takes several hours, making its application more expensive and would be decisive for the operating time of the purification process in which it is introduced. However, it is important to note that no residual hazards are generated during its application, and the material can be eluted to be used in several removal cycles.

In photodegradation, the process becomes more expensive due to the use of electrical energy that this technique requires, in addition to obtaining a by-product that, although its concentration under the conditions described in work, is not alarming, its concentration in the remaining solution constitutes an additional parameter to be measured during the process.

555 Furthermore, high pollutant removal values are achieved with this technique, especially if
556 radicals are used in the process, which is also an element to consider because it represents an
557 additional cost in reagents for the technique.
558
559 **4. Conclusions**
560
561 The adsorption of TCS in an aqueous solution on AC was studied. The textural
562 properties experiments showed that the specific area of the AC is relatively high because they
563 are constituted mainly by micropores. This behavior was confirmed by nitrogen
564 physisorption analysis. The PZC values for the activated carbons were 6.00 for the Darco,
565 8.75 for the Norit, and 8.25 for the F400. Kinetic experiments demonstrated that the
566 diffusional model shows a good fit to the TCS concentration as a function of time.
567 Furthermore, the intensity of the adsorption and the pH of the solution are closely related.
568 The results of the direct and radical photodegradation tests make it possible to ensure
569 that the triclosan molecule is sensitive to UV light of 254 nm. Using a radical generator such
570 as potassium persulfate can increase photodegradation efficiency at high concentrations. It
571 was possible to identify 2,4-dichlorophenol as one of the photolytic degradation products of
572 triclosan. This compound was quantified, resulting in its concentration being much lower
573 than that of triclosan, and it does not represent an environmental hazard at low concentrations
574 of triclosan in water. According to the literature consulted, the rest of the products obtained
575 are safe.

Acknowledgments

National Council of Science and Technology, CONACyT, Mexico. Grant 755931; PN-3947-2016 and CB-286990-2016.

References

Allmyr M, Adolfsson-Erici M, McLachlan MS, Sandborgh-Englund G (2006a) Triclosan in plasma and milk from Swedish nursing mothers and their exposure via personal care products. Sci Total Environ 372:87–93

Allmyr M, McLachlan MS, Sandborgh-Englund G, Adolfsson-Erici M (2006b) Determination of triclosan as its pentafluorobenzoyl ester in human plasma and milk using electron capture negative ionization mass spectrometry. Anal Chem 78:6542–6546

Andrade SN, Veloso CM, Fontan RCI, et al (2018) Chemical-activated carbon from coconut (Cocos nucifera) endocarp waste and its application in the adsorption of ß-lactoglobulin protein. Rev Mex Ing Química 17:463–475

Babić BM, Milonjić SK, Polovina MJ, Kaludierović B V (1999) Point of zero charge and intrinsic equilibrium constants of activated carbon cloth. Carbon N Y 37:477–481

Behera SK, Oh S-Y, Park H-S (2010) Sorption of triclosan onto activated carbon, kaolinite and montmorillonite: effects of pH, ionic strength, and humic acid. J Hazard Mater 179:684–691

Boehm HP (1994) Some aspects of the surface chemistry of carbon blacks and other carbons.

598 Carbon N Y 32:759–769
599 Calafat AM, Ye X, Wong L-Y, et al (2007) Urinary concentrations of triclosan in the US
600 population: 2003–2004. Environ Health Perspect 116:303–307
601 Carrales-Alvarado DH, Ocampo-Pérez R, Leyva-Ramos R, et al (2016) Removal of the
602 antibiotic metronidazole by adsorption on various carbon materials from aqueous phase.
603 J Colloid Interface Sci 22:276–285
604 Carrott PJM, Nabais JM V, Carrott MMLR, Menéndez JA (2001) Thermal treatments of
605 activated carbon fibres using a microwave furnace. Microporous Mesoporous Mater
606 47:243–252
607 Cho E-J, Kang J-K, Moon J-K, et al (2021) Removal of triclosan from aqueous solution via
608 adsorption by kenaf-derived biochar: Its adsorption mechanism study via spectroscopic
609 and experimental approaches. J Environ Chem Eng 9:106343
610 Citraningrum CHM, Gunawan NI, Ismadji S (2007) The Influence of Thermal Modification
611 and pH of Solution to the Adsorption of Phenol onto NORIT Granular Activated Carbon
612 El-Sayed Y, Bandosz TJ (2004) Adsorption of valeric acid from aqueous solution onto
613 activated carbons: role of surface basic sites. J Colloid Interface Sci 273:64–72
614 Ensley HE, Barber JT, Polito MA, Oliver AI (1994) Toxicity and metabolism of 2, 4-
615 dichlorophenol by the aquatic angiosperm Lemna gibba. Environ Toxicol Chem An Int
616 J 13:325–331
617 Fiol N, Villaescusa I (2009) Determination of sorbent point zero charge: usefulness in
618 sorption studies. Environ Chem Lett 7:79–84
619 Franz S, Altenburger R, Heilmeier H, Schmitt-Jansen M (2008) What contributes to the
620 sensitivity of microalgae to triclosan? Aquat Toxicol 90:102–108

621 Freundlich HMF (1906) Over the adsorption in solution. J Phys chem 57:1100–1107
622 Furusawa T, Smith JM (1973) Fluid-particle and intraparticle mass transport rates in slurries.
623 Ind Eng Chem Fundam 12:197–203
624 González-Fernández LA, Medellín-Castillo NA, Ocampo-Pérez R, et al (2021) Equilibrium
625 and kinetic modelling of triclosan adsorption on Single-Walled Carbon Nanotubes. J
626 Environ Chem Eng 106382. https://doi.org/10.1016/J.JECE.2021.106382
627 Hessler DP, Gorenflo V, Frimmel FH (1993) Degradation of Aqueous Atrazine and
628 Metazachlor Solutions by UV and UV/H2O2—Influence of pH and Herbicide
629 Concentration Abbau von Atrazin und Metazachlor in wäßriger Lösung durch UV und
630 UV/H2O2—Einfluß von pH und Herbizid-Konzentration. Acta Hydrochim Hydrobiol
631 21:209–214
632 Hong M, Yu L, Wang Y, et al (2019) Heavy metal adsorption with zeolites: The role of
633 hierarchical pore architecture. Chem Eng J 359:363–372
634 Kazner C (2011) Advanced wastewater treatment by nanofiltration and activated carbon for
635 high quality water reuse
636 Krijgsheld KR, Van der Gen A (1986) Assessment of the impact of the emission of certain
637 organochlorine compounds on the aquatic environment: Part I: Monochlorophenols and
638 2, 4-dichlorophenol. Chemosphere 15:825–860
639 Langmuir I (1918) The adsorption of gases on plane surfaces of glass, mica and platinum. J
640 Am Chem Soc 40:1361–1403
641 Latch DE, Packer JL, Arnold WA, McNeill K (2003) Photochemical conversion of triclosan
642 to 2, 8-dichlorodibenzo-p-dioxin in aqueous solution. J Photochem Photobiol A Chem
643 158:63–66

644 Lemaire J, Campbell I, Hulpke H, et al (1982) An assessment of test methods for
645 photodegradation of chemicals in the environment. Chemosphere 11:119–164
646 Leyva-Ramos R, Diaz-Flores PE, Leyva-Ramos J, Femat-Flores RA (2007) Kinetic
647 modeling of pentachlorophenol adsorption from aqueous solution on activated carbon
648 fibers. Carbon N Y 45:2280–2289
649 Leyva-Ramos R, Geankoplis CJ (1985) Model simulation and analysis of surface diffusion
650 of liquids in porous solids. Chem Eng Sci 40:799–807
651 Liang C, Wang Z-S, Mohanty N (2006) Influences of carbonate and chloride ions on
652 persulfate oxidation of trichloroethylene at 20 C. Sci Total Environ 370:271–277
653 Lopez-Ramon MV, Stoeckli F, Moreno-Castilla C, Carrasco-Marin F (1999) On the
654 characterization of acidic and basic surface sites on carbons by various techniques.
655 Carbon N Y 37:1215–1221
656 Maffei AV, Budd PM, McKeown NB (2006) Adsorption studies of a microporous
657 phthalocyanine network polymer. Langmuir 22:4225–4229
658 Marazuela MD, García-Fresnadillo D (2020) An integrated photosensitizing/adsorbent
659 material for the removal of triclosan from water samples. Sep Purif Technol 251:117392
660 Medellin-Castillo NA, Ocampo-Pérez R, Leyva-Ramos R, et al (2013) Removal of diethyl
661 phthalate from water solution by adsorption, photo-oxidation, ozonation and advanced
662 oxidation process (UV/H2O2, O3/H2O2 and O3/activated carbon). Sci Total Environ
663 442:26–35
664 Mezcua M, Gómez MJ, Ferrer I, et al (2004) Evidence of 2, 7/2, 8-dibenzodichloro-p-dioxin
665 as a photodegradation product of triclosan in water and wastewater samples. Anal Chim
666 Acta 524:241–247

667 Mohanty K, Das D, Biswas MN (2006) Preparation and characterization of activated carbons
668 from Sterculiaalata nutshell by chemical activation with zinc chloride to remove phenol
669 from wastewater. Adsorption 12:119–132
670 Moore JW, Ramamoorthy S (2012) Heavy metals in natural waters: applied monitoring and
671 impact assessment. Springer Science & Business Media
672 Moreno-Pérez J, Pauletto PS, Cunha AM, et al (2021) Three-dimensional mass transport
673 modeling of pharmaceuticals adsorption inside ZnAl/biochar composite. Colloids
674 Surfaces A Physicochem Eng Asp 614:126170
675 MØRETRØ T, Sonerud T, MANGELROeD E, Langsrud S (2006) Evaluation of the
676 antibacterial effect of a triclosan-containing floor used in the food industry. J Food Prot
677 69:627–633
678 Nfodzo P, Choi H (2011) Triclosan decomposition by sulfate radicals: Effects of oxidant and
679 metal doses. Chem Eng J 174:629–634. https://doi.org/10.1016/j.cej.2011.09.076
680 Ocampo-Pérez R, Rivera-Utrilla J, Méndez-Díaz JD, Sánchez-Polo M (2012) Modeling
681 adsorption rate of organic micropollutants present in landfill leachates onto granular
682 activated carbon. J Colloid Interface Sci 385:174–182
683 Pauletto PS, Moreno-Pérez J, Hernández-Hernández LE, et al (2021) Novel biochar and
684 hydrochar for the adsorption of 2-nitrophenol from aqueous solutions: An approach
685 using the PVSDM model. Colloids Surfaces A Physicochem Eng Asp 614:126170
686 Pauletto PS, Moreno-Pérez J, Hernández-Hernández LE, et al (2020) Interpretations on the
687 mechanism of In (III) adsorption onto chitosan and chitin: A mass transfer model
688 approach. J Mol Liq 304:112758
689 Perez-Cadenas AF, Maldonado-Hodar FJ, Moreno-Castilla C (2003) On the nature of surface

690 acid sites of chlorinated activated carbons. Carbon N Y 41:473–478
691 Radke CJ, Prausnitz JM (1972) Adsorption of organic solutes from dilute aqueous solution
692 of activated carbon. Ind Eng Chem Fundam 11:445–451
693 Rainbow PS (2006) Biomonitoring of trace metals in estuarine and marine environments.
694 Australas J Ecotoxicol 12:107–122
695 Rainbow PS (1995) Biomonitoring of heavy metal availability in the marine environment.
696 Mar Pollut Bull 31:183–192
697 Rivera-Utrilla J, Sánchez-Polo M (2002) Ozonation of 1, 3, 6-naphthalenetrisulphonic acid
698 catalysed by activated carbon in aqueous phase. Appl Catal B Environ 39:319–329
699 Segovia-Sandoval SJ, Padilla-Ortega E, Carrasco-Marín F, et al (2019) Simultaneous
700 removal of metronidazole and Pb (II) from aqueous solution onto bifunctional activated
701 carbons. Environ Sci Pollut Res 26:25916–25931
702 Singer H, Müller S, Tixier C, Pillonel L (2002) Triclosan: occurrence and fate of a widely
703 used biocide in the aquatic environment: field measurements in wastewater treatment
704 plants, surface waters, and lake sediments. Environ Sci Technol 36:4998–5004
705 Son H-S, Choi S-B, Zoh K-D, Khan E (2007) Effects of ultraviolet intensity and wavelength
706 on the photolysis of triclosan. Water Sci Technol 55:209–216
707 Son H, Khim J, Zoh K (2010) Degradation of triclosan in the combined reaction of Fe2+ and
708 UV-C: Comparison with the Fenton and photolytic reactions. Environ Prog Sustain
709 Energy 29:415–420
710 Sotiropoulou REP, Serafidou M, Skodras G (2019) Effect of oxygen functional groups on
711 mercury retention in activated carbons
712 Wang S-L, Tzou Y-M, Lu Y-H, Sheng G (2007) Removal of 3-chlorophenol from water

using rice-straw-based carbon. J Hazard Mater 147:313–318

Wang S, Wang J (2019) Activation of peroxymonosulfate by sludge-derived biochar for the degradation of triclosan in water and wastewater. Chem Eng J 356:350–358

Xu M, Zhang H, Guégan F, et al (2020) Activated charcoal grafted with phenyl imidazole groups for Knoevenagel condensation of furfural with malononitrile. Catal Commun 147:106151

Zdravkov BD, Čermák JJ, Šefara M, Janků J (2007) Pore classification in the characterization of porous materials: A perspective. Cent Eur J Chem 5:385–395

Statements and Declarations

The authors declare the following financial interests/personal relationships which may be considered as potential competing interests: Nahum Andres Medellin Castillo reports financial support was provided by Consejo Nacional de Ciencia y Tecnología (CONACyT) CB 286990 2016 and PN 3947 2016.

Competing Interests

The authors have no relevant financial or non-financial interests to disclose.

CRediT author statement

Lázaro Adrián González-Fernández: Conceptualization, Methodology, Software, Validation, Formal Analysis, Investigation, Data Curation, Writing-Original Draft, Visualization.

Nahum Andrés Medellín-Castillo: Conceptualization, Methodology, Software, Validation, Formal Analysis, Investigation, Writing-Original Draft, Resources, Supervision. **Raúl Ocampo-Pérez**: Conceptualization, Methodology, Software, Validation, Formal Analysis, Investigation, Resources, Supervision. **Roberto Leyva-Ramos:** Conceptualization, Supervision, Formal Analysis, Writing-Original Draft. **Guilherme Luiz-Dotto:** Conceptualization, Supervision, Writing-Original Draft. **Rogelio Flores-Ramírez:** Conceptualization, Supervision. **Amado Enrique Navarro Frómeta:** Conceptualization, Supervision, Writing-Original Draft. **Miguel Mauricio Aguilera-Flores:** Conceptualization. **Francisco Carrasco Marín:** Conceptualization, Supervision. ***Héctor Hernández-Mendoza****:* Conceptualization, Supervision. **Samuel Aguirre-Contreras**: Conceptualization, Software.